Applied Catalysis B: Environmental 142–143 (2013) 129–141

Contents lists available at SciVerse ScienceDirect

Applied Catalysis B: Environmental

journal homepage: www.elsevier.com/locate/apcatb

Ozone initiated dechlorination and degradation of trichlorophenol using Ce–Zr loaded metal oxides as catalysts

Suresh Maddila, Venkata D.B.C. Dasireddy, Ekemena O. Oseghe, Sreekanth B. Jonnalagadda*

School of Chemistry, University of KwaZulu-Natal, Westville Campus, Chiltern Hills, Durban 4000, South Africa

ARTICLE INFO

Article history:
Received 19 February 2013
Received in revised form 3 May 2013
Accepted 8 May 2013
Available online 15 May 2013

Keywords:
Trichlorophenol
Ozone
Cerium–Zirconium oxide
Titania
Dihydroxyfumaric acid

ABSTRACT

Oxidative dechlorination and degradation of trichlorophenol (TCP) in aqueous system initiated by ozone and catalyzed by varied loadings of cerium–zirconium oxide on metal oxides supports namely; Al_2O_3, SiO_2 and TiO_2 was investigated. Catalyst materials were synthesized and characterized by using various surface characterization techniques including XRD, BET, TPD, ICP, SEM, TEM and FT-IR. XRD showed that cerium–zirconia exists as three different phases on the surface of the catalysts. SEM and SEM–EDX indicated that cerium–zirconia oxide is well dispersed on the surface of the TiO_2 with compared to Al_2O_3 and SiO_2 supports. TEM showed that particle size of Ce–Zr is in the range of 40–80 nm. Catalyst testing was done as function of reaction time and pH in a semi batch reactor. The oxidation products formed in the reaction were characterized by IR, ^{1}H NMR and LC–MS mass spectral data. Dihydroxyfumaric acid (DHFA) and oxalic acid (OA) were the main oxidation products. The product distribution was dependent on the acidic character of the catalysts. Among the catalysts tested, 2.5% Ce–Zr/SiO_2 showed good activity with 100% conversion in 4 h while others needed 5 h.

1. Introduction

Ozonation is very effective in treating wastewaters containing chlorophenolic compounds [1,2] and is widely used in water treatment throughout the world including for effective microbial disinfection [3]. One of its strengths is its oxidation potential, for example in decoloration and in elimination of refractory pollutants [4–6]. Molecular ozone is a powerful oxidant and is selective, but it reacts reaction with some organic compounds is slow. Fortunately, it is unstable in water and decomposes into hydroxyl radicals and reacts rapidly with a number of species [5,6].

Ozonation of water, mainly drinking water, has been studied since about 1850. Over the past few decades, scope of ozonation in water treatment, including water containing different dissociated or non-dissociated, organic or inorganic compounds has received more attention [1,7–9]. Although ozone has a higher oxidation potential than chlorine compounds [10], molecular ozone reacts only selectively with nucleophilic molecules. Contrary to molecular ozone, the •OH radical, which is the product of ozone decomposition and one of the most reactive agents, reacts non-selectively with almost all kinds of substances [11,12]. Ozone forms •OH radicals through decomposition reactions with —OH ions or dissociated hydrogen peroxide. The formation of hydrogen peroxide during the ozonation of various organic compounds was observed [13]. Various intermediate radicals provide the establishment of radical chain reactions leading to ·OH [14,15]. All radicals can be scavenged by combination with other radicals or through production of secondary radicals with low reactivity. The most important scavengers in wastewater are carbonate and bicarbonate. When the ozonation is used in the treatment of industrial wastewater [16], the initiation of the radical chain through —OH ions and its promotion through H^+ does not allow a simple separation of the complex reaction scheme into pure ·OH radical or molecular ozonolysis regimes by varying the pH of the reactant solution [17,18].

Chlorinated organic compounds are widely used and can found in nearly all major environmental compartments. Chlorophenols have a wide range of wood preservatives, industrial and domestic uses, and they are employed as industrial solvents or intermediates in the synthesis of other chemicals, dyestuffs, pesticides, lubricants and dielectric [19–21]. Chlorophenols are among the hazardous pollutants found in various waste oils. They are highly toxic, mutagenic and possibly carcinogenic. Furthermore, chlorophenols are bio refractory and once released into ecosystems over a period of time tend to accumulate in animal tissue [22–24]. This raises an urgent need for efficient dechlorination methods to eliminate chloro functionalities from both concentrated and diluted industrial effluents which pollute the ground water [25].

* Corresponding author. Tel.: +27 31 260 7325; fax: +27 31 260 3091.
E-mail address: jonnalagaddas@ukzn.ac.za (S.B. Jonnalagadda).

0926-3373/$ – see front matter © 2013 Elsevier B.V. All rights reserved.
http://dx.doi.org/10.1016/j.apcatb.2013.05.012

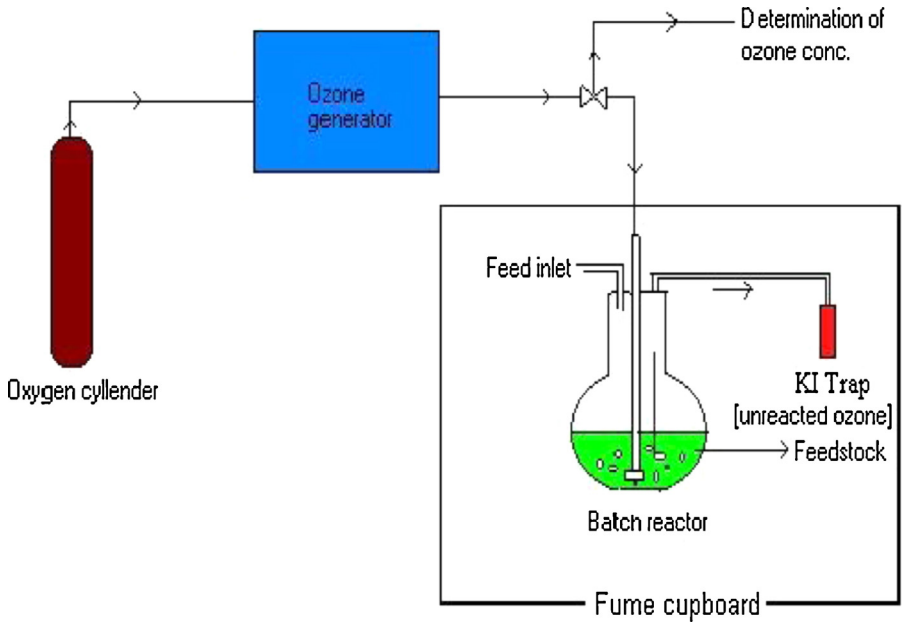

Fig. 1. Dimensions of reactor used in ozonation reactions.

The use of heterogeneous catalysts and ozonation, in the form of advanced oxidation processes in treatment of industrial effluents has significantly increased [26]. Heterogeneous catalysts with good stability and lower losses improve the efficiency of ozone decomposition, as catalyst materials can be recycled/reused without further treatment. Due to these advantages, the heterogeneous catalysts are widely used. The efficiency of the catalytic ozonation process depends to a great extent on the catalyst and its surface properties as well as the pH of the solution that influences the properties of the surface active sites and ozone decomposition reactions in aqueous solutions [27]. The most important factor for heterogeneous system is the choice of catalysts. Now, the commonly studied catalysts are metal oxides, and metals or metal oxides on supports. Bimetallic loaded catalysis, in which the presence of two metal components leads to a synergistic behavior which makes catalysts more effective with maximum durability. Due to the metal loading and a preparation technique i.e. wet impregnation provides a sophisticated level of results with compared to conventional preparation methods.

The aim of current study is to investigate the role of low cost bi-metallic catalysts in the oxidation of chlorophenolic aqueous solutions by means of a coupled heterogeneous system. This material has been tested successfully for ozonation processes. Besides the assessment of the benefits of the heterogeneous catalytic peroxide oxidation, multivariate analysis has been used to study the conditions (oxidant and catalyst concentrations) that yield the best results in terms of organic degradation and catalyst stability.

2. Materials and methods

2.1. Ozonolysis experiment

Ozone was generated using a Fischer Ozone 500 generator, which produced ozone by the electric discharge of oxygen from a compressed oxygen cylinder via the corona discharge method. Ozone gas was bubbled into a 50 cm^3 reactor through a sintered porous diffuser with porosity 2. All the ozone aeration experiments were carried out under the controlled conditions of room temperature (20 ± 1) °C using 20 mL 10% (w/v) of trichlorophenol (TCP) in water at fixed ozone concentration (0.05 M) and flow rate of 100 ml/min for 5 h. Fig. 1 illustrates the dimensions of the semi-batch reactor used. A magnetic stirrer placed at the bottom of the reaction vessel was used to ensure maximum contact of the substrate with ozone by continuous stirring. The amount of ozone was estimated by volumetric method trapping it in KI solution and titrating the liberated iodine using standard thiosulfate solution with starch as indicator [28]. Flow rates and ozone concentrations were calibrated and highly reproducible. Parameters were checked in duplicate runs, prior to and after each of the experiments. Results were highly reproducible and with less than 5% difference. Where difference was greater, such experiments replicated and data with less than 5% differences were only considered. As most of the experiments were done only in duplication, statistical analysis of the results could not be undertaken. In all cases although differences were small, trends were consistent, hence cautions approach is taken while comparing the results.

2.2. Catalyst preparation

The catalysts were prepared by wet impregnation method by dissolving appropriate amount of Ce [$Ce(NO_3)_2{\cdot}3H_2O$, Aldrich-99%, 0.1–0.3 g], Zr [$Zr(NO_3)_2{\cdot}5H_2O$, Aldrich-99%, 0.1–0.3 g] in distilled water [40.0 mL] and adding it to 10 g of γ-alumina [γ-Al_2O_3, Aldrich], titania [TiO_2, Aldrich] and silica [SiO_2, Aldrich] stirring for 3 h using a magnetic stirrer at room temperature and again at room temperature for overnight. Catalysts are further dried in an oven at 130–140 °C for 12 h. Then the catalysts are calcined in the presence of air, at 550 °C for 3 h to obtain the 1% and 2.5% (w/w) catalysts [28–30].

2.3. Instrumentation

2.3.1. Textural properties

The Brunauer–Emmett–Teller (BET) surface area, total pore volume and average pore size were measured using a Micrometrics Tristar II surface area and porosity analyzer. Prior to the analysis, the powdered samples (~0.180 g) were degassed under N_2 for 12 h at 200 °C using a Micromeritics Flow Prep 060 instrument.

Textural properties of catalyst samples were measured by N_2 adsorption–desorption isotherms obtained at −196 °C.

2.3.2. Temperature programmed desorption (TPD)

In the TPD experiments, the catalyst was pretreated at 350 °C under the stream of helium for 60 min. The temperature was then decreased to 80 °C. A mixture of 5% ammonia in helium was passed over the catalyst at a flow rate of 30 mL/min for 60 min. The excess ammonia was removed by purging with helium for 30 min. The temperature was then raised gradually to 950 °C by ramping at 10 °C/min under the flow of helium and desorption data was recorded.

2.3.3. Inductively coupled plasma-optical emission spectroscopy (ICP-OES)

The actual metal loading was determined by using Perkin Elmer Inductively coupled plasma Optical Emission Spectrometer (ICP-OES) Optima 5300 DV. Samples were solubilized in aqua regia and homogenized by a microwave digestion process, prior to ICP analysis.

2.3.4. Scanning electron microscopy

The SEM measurements were carried out using a JEOL JSM-6100 microscope equipped with an energy-dispersive X-ray analyzer (EDX). The images were taken with an emission current = 100 μA by a tungsten (W) filament and an accelerator voltage = 12 kV. The catalysts were secured onto brass stubs with carbon conductive tape, sputter coated with gold and viewed in JEOL JSM-6100 microscope. The pre-treatment of the samples consisted of coating with an evaporated Au film in a Polaron SC 500 Sputter Coater metallizator to increase the catalyst electric conductivity.

2.3.5. Transmission electron microscopy

The TEM images were viewed on a JEOL JEM-1010 electron microscope. The images were captured and analyzed by using iTEM software. High resolution TEM images were recorded by using JEOL JEM 2100 Electron Microscope.

2.3.6. X-ray diffraction (XRD) analysis

Different metal oxide phases in the catalysts were observed using powder X-ray diffraction (XRD) performed on a Bruker D8 Advance instrument, equipped with an Anton Paar XRK 900 reaction chamber, a TCU 750 temperature control unit and a Cu Kα radiation source with a wavelength of 1.5406 nm at 40 kV and 40 mA. Diffractograms were recorded over the 2θ scale range of 15–90° with a step size of 0.02 s^{-1}.

2.3.7. GC–MS analysis

In all the experiments the organic layer was extracted by using 3× 5.0 mL diethyl ether in a separating funnel and excess water was removed by the addition of anhydrous sodium sulfate (Na_2SO_4). The product was filtered and the solvent was allowed to evaporate. The product was characterized by GC–MS. The amount of TCP consumed in the reaction is expressed as a percentage of original amounts and it refers to reaction conversion. Selectivity refers to the amount of product formed divided by the reactant consumed.

2.3.8. ^{1}H NMR and LC–MS

^{1}H NMR (400 MHz) spectra were recorded on a Bruker AMX 400 MHz NMR spectrometer in $CDCl_3$/DMSO-d_6 solution using TMS as an internal standard. All chemical shifts are reported in δ (ppm) using TMS as an internal standard. The mass spectra were recorded on an Agilent 1100 LC/MSD instrument, with method API-ES, at 70 eV.

Table 1
BET surface area, elemental analysis and TPD data of Ce–Zr loaded supports.

Catalyst	ICP (wt%)		Surface area (m^2/g)	Pore volume (cm^3/g)	Pore diameter (Å)	EDX (wt%)		Acidity (mmol NH_3/g)	Specific acidity (mmol NH_3/m^2)
	Ce	Zr				Ce	Zr		
Al_2O_3	–	–	251	0.98	125	–	–	920	4.27
1%Ce–Zr/Al_2O_3	0.48	0.47	207	0.56	90	0.45	0.41	815	3.93
2.5% Ce–Zr/Al_2O_3	1.20	1.22	187	0.50	91	1.05	1.12	725	3.87
SiO_2	–	–	210	0.75	189	–	–	3600	17.14
1% Ce–Zr/SiO_2	0.49	0.48	275	1.055	151	0.38	0.31	2450	10.25
2.5% Ce–Zr/SiO_2	1.24	1.25	239	0.93	150	1.00	1.11	2140	8.95
TiO_2	–	–	88	0.42	115	–	–	620	7.04
1% Ce–Zr/TiO_2	0.44	0.48	123	0.34	108	0.37	0.41	541	4.39
2.5% Ce–Zr/TiO_2	1.22	1.24	111	0.33	97	1.11	1.12	422	3.81

2.3.9. FT-IR analysis

FT-IR spectra of various catalyst samples were recorded on a Nicolet Impact 400 equipment and Nicolet Impact Model-420 spectrometer with a 4 cm^{-1} resolution and 128 scans in the mid IR (400–4000 cm^{-1}) region using the KBr pellet technique. About 100.0 mg of dry KBr was mixed with a little amount (10.0 mg) of the sample and was ground for homogenization. During the mixing an IR lamp was used for drying. The mixture was then pressed into a transparent, thin pellet at 10 tons cm^{-2}. These pellets were used for the IR spectral measurements.

3. Results and discussion

3.1. BET surface area and elemental analysis (BET and ICP)

The surface areas and the elemental composition for the catalysts are shown in Table 1. The Ce and Zr wt% obtained from ICP are in correlation with the nominal weight loading. SEM–EDX data also showed presence of Ce and Zr in the catalysts with the appropriate nominal loading on the surface of the supports. In order to understand the pore structure of the catalysts, the N_2 adsorption–desorption measurements were carried out. The corresponding N_2 adsorption–desorption distribution isotherms of the catalysts are shown in Fig. 2. All the isotherms showed the hysteric loop (Type IV-IUPAC) which demonstrates the presence of mesoporous character in all the catalysts [31,32]. Surface area and the pore volume of the catalysts decreased with the cerium–zirconium loading. This could be attributed to the clogging of the narrow pores of the support with the cerium–zirconium making it inaccessible to nitrogen molecules, leading to a decrease in the surface area. The Ce–Zr loaded on Al_2O_3 and TiO_2 support material exhibited a lower surface area than silica supported catalysts this is due to the surface area contribution from the SiO_2 support and due to the weak interaction between the Ce–Zr and, Ce–Zr particles may be

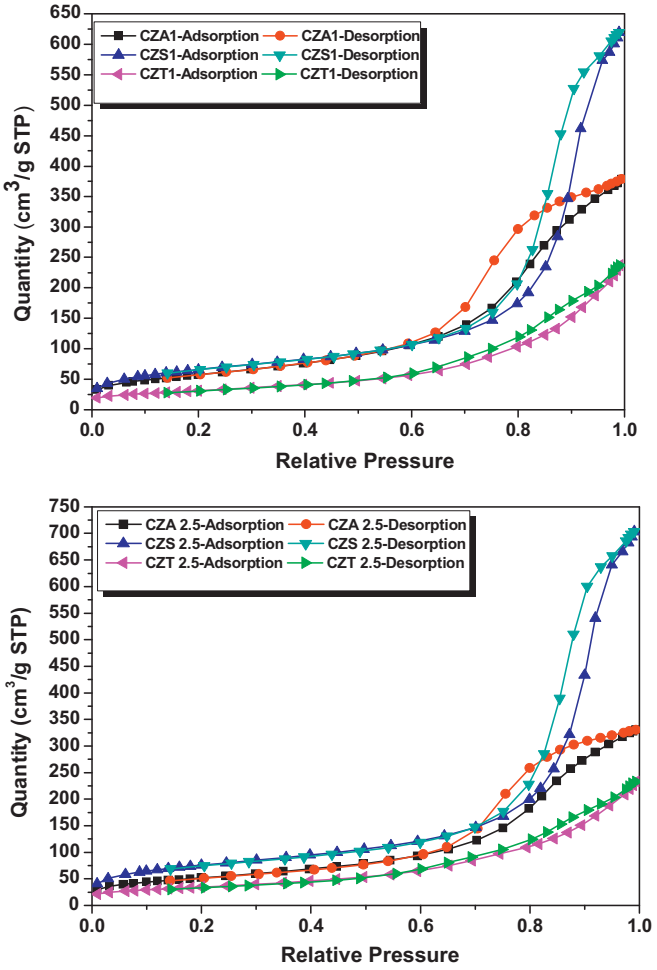

Fig. 2. N_2 adsorption–desorption isotherms of catalysts.

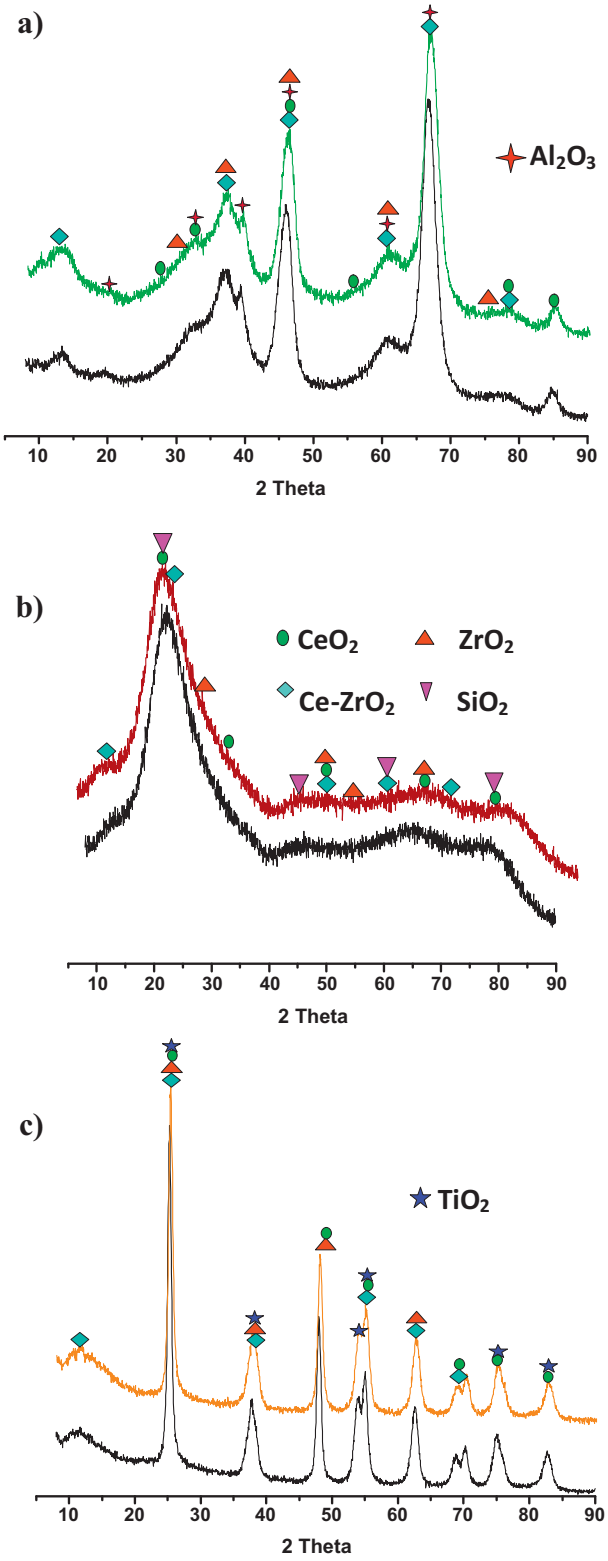

Fig. 3. XRD spectra: (a) 1 and 2.5% Ce–Zr loaded on Al_2O_3. (b) 1 and 2.5% Ce–Zr loaded on SiO_2. (c) 1 and 2.5% Ce–Zr loaded on TiO_2.

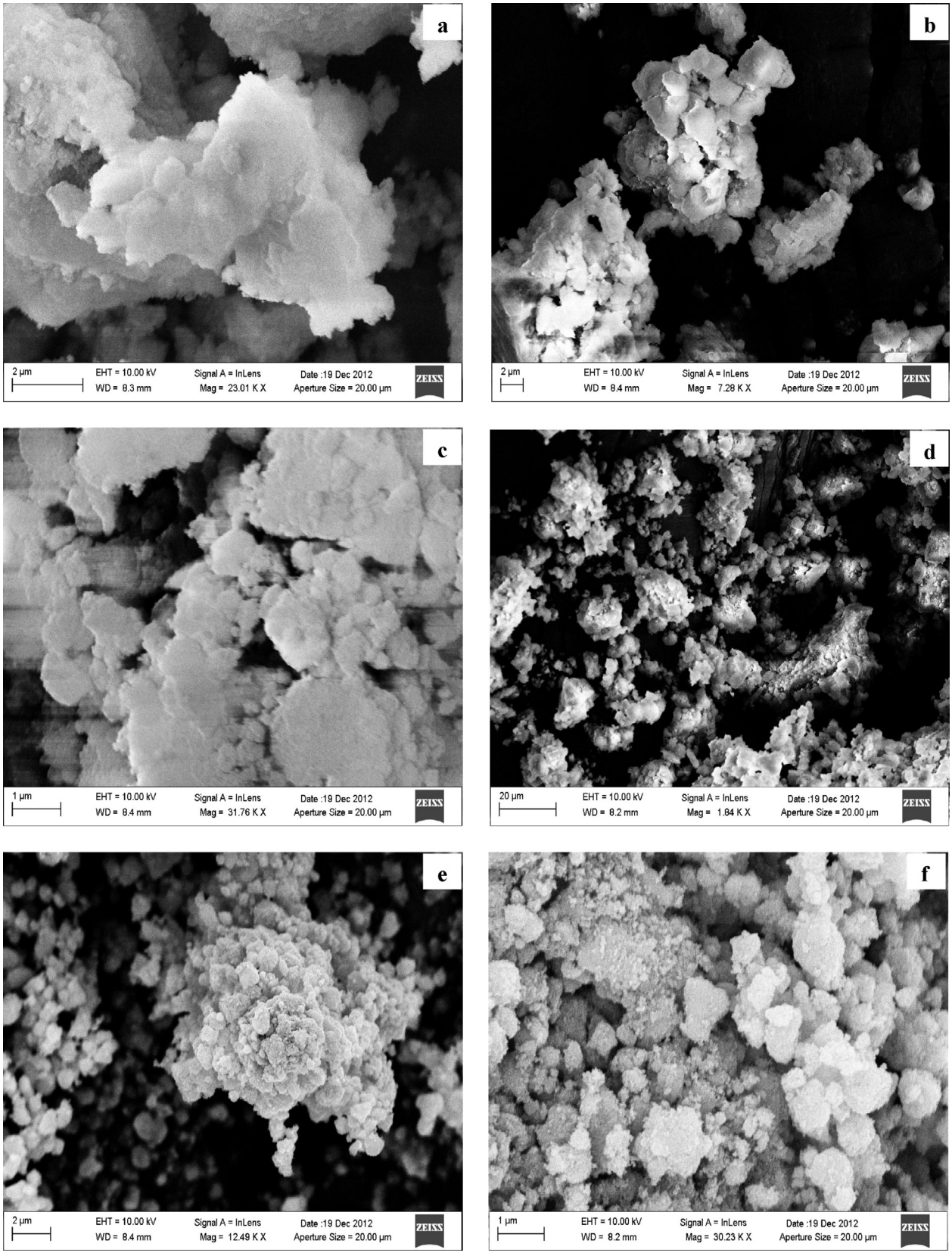

Fig. 4. SEM images: (a and b) 1% and 2.5% Ce–Zr on Al_2O_3. (c and d) 1% and 2.5% Ce–Zr on SiO_2. (e and f) 1% and 2.5% Ce–Zr on TiO_2.

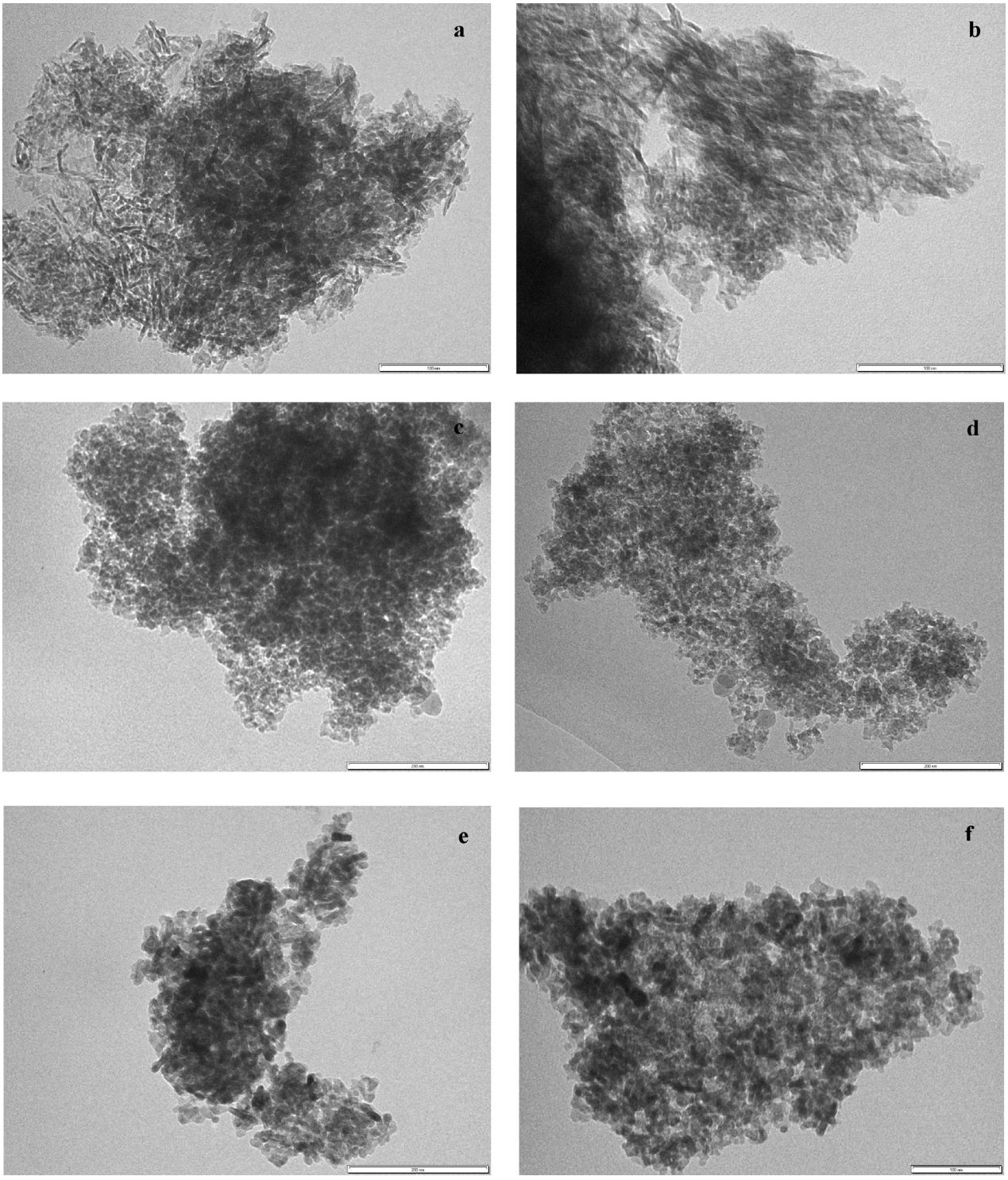

Fig. 5. TEM images: (a and b) 1% and 2.5% Ce–Zr on Al_2O_3. (c and d) 1% and 2.5% Ce–Zr on SiO_2. (e and f) 1% and 2.5% Ce–Zr on TiO_2.

agglomerated on the surface of the SiO_2. The surface areas for the catalysts are shown in Table 1. The catalysts showed the small range of pore diameter along with high pore volumes and surface area, which demonstrates the mesoporus character of the catalysts. The mesoporous size has significant role on the adsorption properties of reactant molecules and thereby it can play a major role in the activity. All catalysts exhibited broad pore size distribution peaks due to the wide range of pore distribution formed due to the Ce–Zr loading. The wide range distribution in the pore size may be correlated with the activity exhibited by the catalysts.

3.2. X-ray diffraction (XRD)

The X-ray diffraction patterns of catalysts with 1 wt% and 2.5 wt% Ce–Zr loaded on Al_2O_3, SiO_2 and TiO_2 are shown in Fig. 3. The phases of supports i.e. alumina, silica and titania are correlating with literature [32,33]. The *d*-spacing's of ceria and zirconia phases are in agreement with the ICDD files no's 01-078-0047, 01-73-6328, 38-1436 for CeO_2, ZrO_2 and Ce–ZrO_2 respectively. There is an evidence of the mixed metal oxide phase i.e. Ce_{50}–$Zr_{50}O_2$, where *d*-spacing's are in correlation with ICDD file no: 28-0271. All

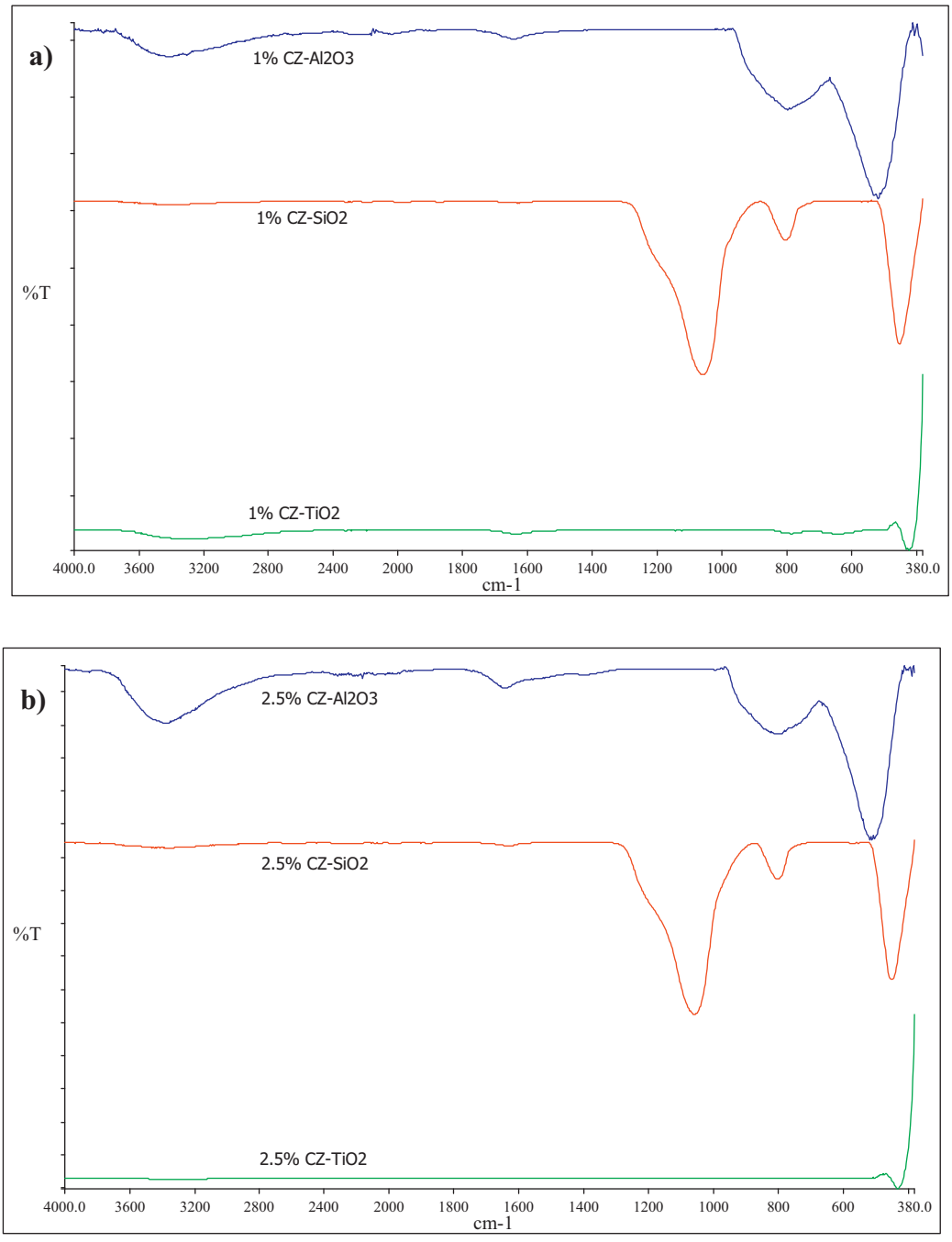

Fig. 6. IR spectra of Ce–Zr loaded on AlO_3, SiO_2 and TiO_2 supports. (a) 1% Ce–Zr loaded. (b) 2.5% Ce–Zr loaded.

catalysts showed the polycrystalline nature, and the crystallinity of all catalysts increases with the increase in the Ce–Zr wt% loadings. Among all the catalysts Ce–Zr supported on TiO_2 catalysts exhibited high crystalline nature.

3.3. Scanning electron microscopy (SEM)

Fig. 4a–f shows the SEM images of the Ce–Zr supported on alumina, silica and titania catalysts. In the presence of Ce–Zr on Al_2O_3 surface is noticeable in Fig. 4a and becomes more conspicuous in Fig. 4b as it seems to totally occupy the surface of the alumina as observed from Fig. 4c, Ce–Zr is distributed over silica surface. The coverage of the alumina surface by Ce–Zr is increased with increase in the Ce–Zr loading. With increase in the loading i.e. in 2.5% Ce–Zr loading (Fig. 4d) the Ce–Zr particles are closer together and occupy the surface more densely which results the decrease in the surface area which is also showed the same trend in BET results. On TiO_2, Ce–Zr (circle white fluffy substance) is more evenly dispersed on the surface with compared to Al_2O_3. When Ce–Zr loading is increased to 2.5% (Fig. 4f), the Ce–Zr particles are agglomerated on the surface of TiO_2. Wide distribution of small particles over all the support materials is observed with 1% Ce–Zr loading. With an increase from 1 wt% to 2.5 wt% Ce–Zr loading, Al_2O_3 and TiO_2 surfaces seem to be completely covered with Ce–Zr particles. For silica, the Ce–Zr particles are agglomerated on the surface of silica. A possible reason could be that silica has a large surface area and therefore requires more Ce–Zr particles to cover its surface. The SEM images confirm the poly crystalline nature of the all the catalysts, which is not affected by the different loadings of cerium–zirconium. SEM–EDX shows (Table 1)

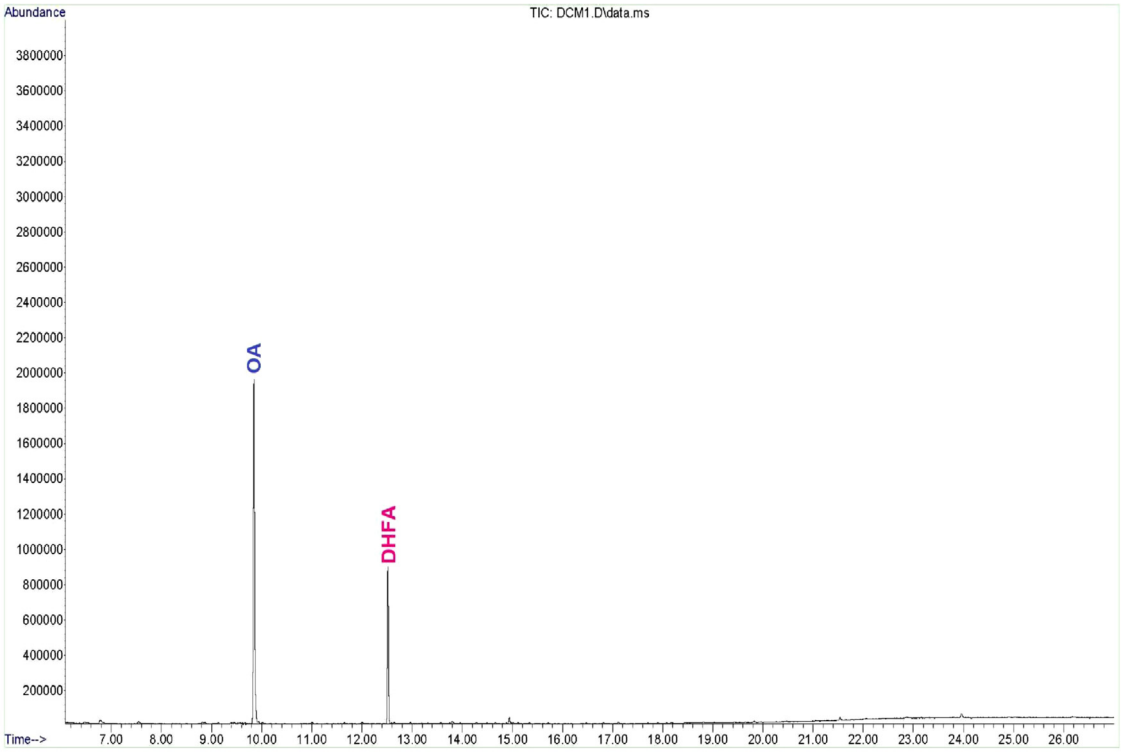

Fig. 7. GC–MS chromatogram of product mixture.

that the cerium–zirconium is evenly distributed on the surface of the supports, and SEM–EDX results are in correlation with ICP-OES elemental analysis.

3.4. Transmission electron microscopy (TEM)

The TEM images of all the catalysts showed an agglomeration of particles on the surface of the supports (Fig. 5). Agglomeration of particles is the result of exposure of the samples to a beam with the high energy resulting in the loss of hydroxyl groups. The agglomeration of the particles is high on the surface of the silica with compared to alumina and titania. On high magnification, the particles appear as irregular a needle-like shape which was also observed in literature [30,33,39]. The darker parts of the images show the presence of Ce–Zr dispersed evenly on the surface which appear as elongated rod-like particles in the TEM images with particle sizes around 40–80 nm. From the TEM images it is evident that that Ce–Zr is dispersed more evenly on the surface of titania with compared to silica and alumina.

3.5. Fourier transform infrared spectroscopy (FT-IR)

A distinct IR absorption bands at 806 and 794 cm^{-1} observed with 1% and 2.5% Ce–Zr/Al_2O_3. The Al_2O_3 peaks are overlapping with the Ce–Zr–O vibrational stretching arising from the presence of Ce–Zr oxides [34,35]. The stretching vibration of hydroxyl groups and also other peaks appeared at 2169 cm^{-1} and 3407 cm^{-1} for 1% Ce–Zr/Al_2O_3 and 2164 cm^{-1} and 3384 cm^{-1} which can be attributed to the adsorbed moisture on the surface of the catalyst (Fig. 6) [34–36]. The spectra show a sharp peak at 521 cm^{-1} and 512 cm^{-1} indicating Ce–O asymmetric stretching vibrations for 1% and 2.5% Ce–Zr/Al_2O_3 respectively. The FT-IR spectrum of 1% and 2.5% Ce–Zr/silica shows bands due to tetrahedral framework vibrations of Si–O–Si linkages at 1063 cm^{-1}. The bands observed at 805 and 803 cm^{-1} due to Ce–Zr–Si–O vibrations, bands at 1630 and 1632 cm^{-1} due to Ce–Zr–O for 1% and 2.5% Ce–Zr/SiO_2 respectively [34–37]. Very weak bands at 3384 cm^{-1} and 3390 cm^{-1} are attributed with acidic bridging hydroxyl groups respectively. The absorption band at 788 and 796 cm^{-1} (Fig. 6a and b) can be attributed to the presence of Ce–Zr/TiO_2. Bands appearing at 518 cm^{-1}, 1124 cm^{-1} for 1% Ce–Zr/TiO_2, and 542 cm^{-1}, 1057 cm^{-1} for 2.5% Ce–Zr/TiO_2 are due to TiO_2. The absorption bands at 1636 cm^{-1} and 1635 cm^{-1} are attributed to Ce–Zr–O peaks, vibrational stretching peaks at 425 cm^{-1} and 434 cm^{-1} are also due to the presence of Ce–O for 1% and 2.5% Ce–Zr/TiO_2 [34–38]. The presence of hydroxyl group on the surface of the catalysts (1% and 2.5% Ce–Zr/TiO_2) is confirmed by absorption bands at 3285 cm^{-1} and 3311 cm^{-1} respectively.

3.6. Catalyst testing and product identification

All the ozonation experiments were conducted by aerating the samples with ozone enriched with oxygen for different times. No reaction occurred with oxygen alone. After ozone aeration, the organic portion of the reaction mixture was extracted and analyzed after every reaction with 60 min intervals. Two products were separated and identified by GC-MS (Fig. 7). Based on the mass spectra and the reference standards, the first oxidation product was confirmed to be dihydroxyfumaric acid (DHFA) and the second product was oxalic acid (OA). The ^{1}P NMR spectrum of DHFA showed a broad singlet for the COOH group at δ 14.23 ppm and singlet at δ 10.29 ppm for the CH group respectively (Supplementary Materials Fig. 1a). IR spectra of DHFA exhibited characteristic absorption bands at 3320, 3082 and 1629 cm^{-1} for the COOH, C—H and C=C stretching vibrations (Supplementary Materials Fig. 1b). The LC–MS mass spectrum showed m/z peak at 149 (M+H) (Supplementary Materials Fig. 1c). Similarly compound OA displayed a broad singlet at δ 13.10 ppm for COOH protons (Supplementary Materials Fig. 2a). The IR spectra of OA exhibited absorption bands at 3444, 3069, and 1890 cm^{-1} corresponding to the stretching frequencies of COOH, CH and C=O groups,

respectively (Supplementary Materials Fig. 2b). Moreover, the LC–MS mass spectrum showed at m/z at 91 (M+H) (Supplementary Materials Fig. 2c). The functional groups observed in the IR, ^{1}H NMR and LC–MS spectrum were in good agreement with spectra corresponding to DHFA and OA. Further, the qualitative test (lime water) confirmed the release of CO_2 during the ozonation reaction and suggested some mineralization of TCP. Ozonation of organic compounds in water is known to produce more biodegradable oxygenated organic products and low molecular weight acids.

3.7. Conversion and selectivity

The ozonation process at acidic, neutral and alkaline pH medium mainly takes place through the direct oxidation of specific functional groups by molecular ozone, which reacts selectively. To optimize the pH of the reaction, ozonation experiments were conducted with 10% (w/v) of trichlorophenol, at pH 3, 7 and 11 in the presence of 1% and 2.5% Ce–Zr oxides on the alumina, silica and titania supports. Similarly, uncatalyzed ozonation was also conducted at acidic, neutral and alkaline pH conditions (Fig. 8a). Uncatalyzed reactions showed improved conversions with increasing pH, which suggests that hydroxyl radicals facilitated the oxidation under alkaline conditions [30,33,39]. A perusal of % conversion data in Fig. 8 indicates that like the uncatalyzed reaction, the optimum pH for DCP degradation for all bimetallic doped catalysts is pH 11, as the reaction under acidic and neutral conditions showed lower conversions. The enhanced conversion under alkaline conditions for the three catalyst supports suggest that in specific terms pH change is not influencing the surface properties of the catalyst, but increasing hydroxyl radical concentration through ozone decomposition. The increase in the rate of hydroxyl radical formation in the presence of O_3 [30,33,39] at higher pH is facilitating the faster oxidation of the substrate. Fig. 8b shows the relation between bimetallic doped catalysts type and % conversion in the ozonation reactions. Most of the 2.5% bimetallic doped catalysts showed 100% conversion in 5 h ozonation time, but the composite material having silica as the support exhibited 100% conversion in 4 h of ozonation time. Fig. 9 also shows the data for % conversion of TCP and selectivity of products over Ce–Zr oxides with alumina, silica and titania support at pH 11. The obtained results indicate that basic pH provides optimal conditions for both the ozone decomposition and for catalyst activity.

3.8. Effect of the metal oxides on support

The activity of supported catalysts depends on the nature of the support. The function of the supported catalysts is able to provide

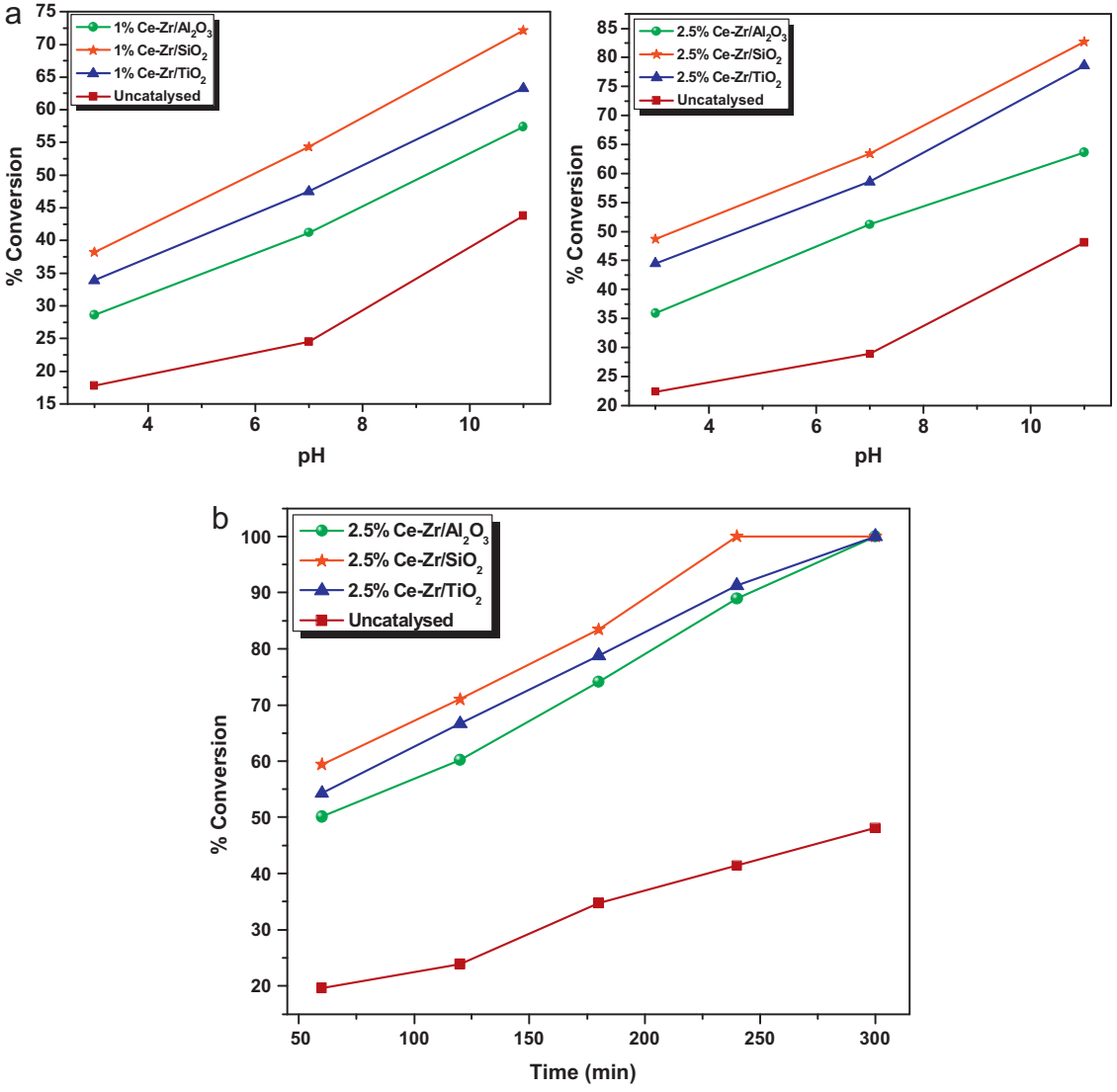

Fig. 8. (a) % conversion of TCP ozonation with different pH. (b) % conversion of TCP with time (min)

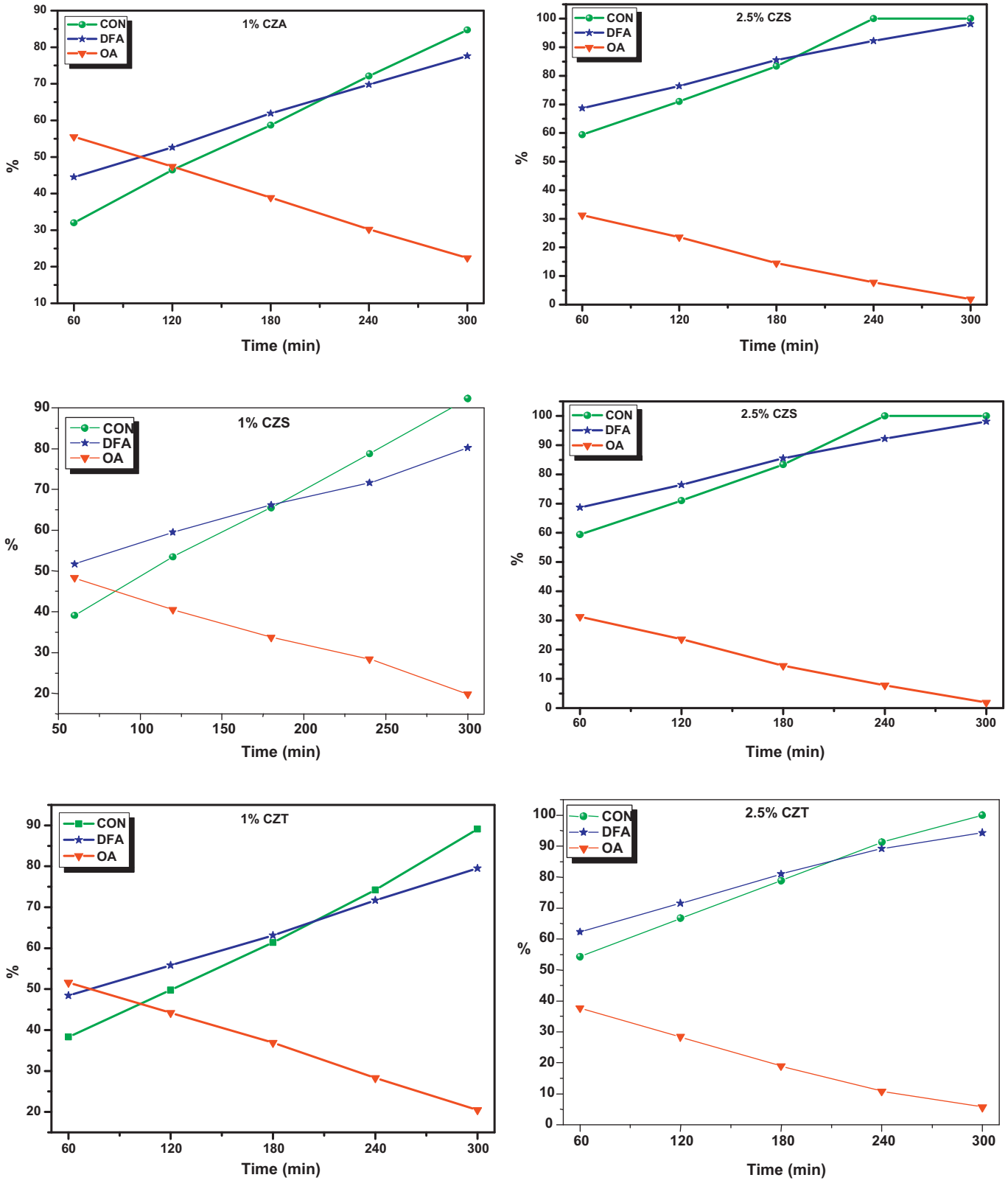

Fig. 9. The conversion and selectivity with 1% and 2.5% loadings of Ce–Zr on metal.

effective surface area and suitable pore structure, make the catalysts to obtain the excellent mechanical strength, thermal stability and play the role of active cite center. In addition, the ordered mesoporous materials with larger surface area are suitable as catalyst support materials. At present, the catalyst supports for the ozonation reactions used widely are Al_2O_3, SiO_2 and TiO_2 and so on [33,40]. In general, the noble metal catalysts have the better catalytic activity than transition metal. However, due to the transition metal is relatively inexpensive, has higher thermal stability and mechanical strength, which lead to transition metal used widely in

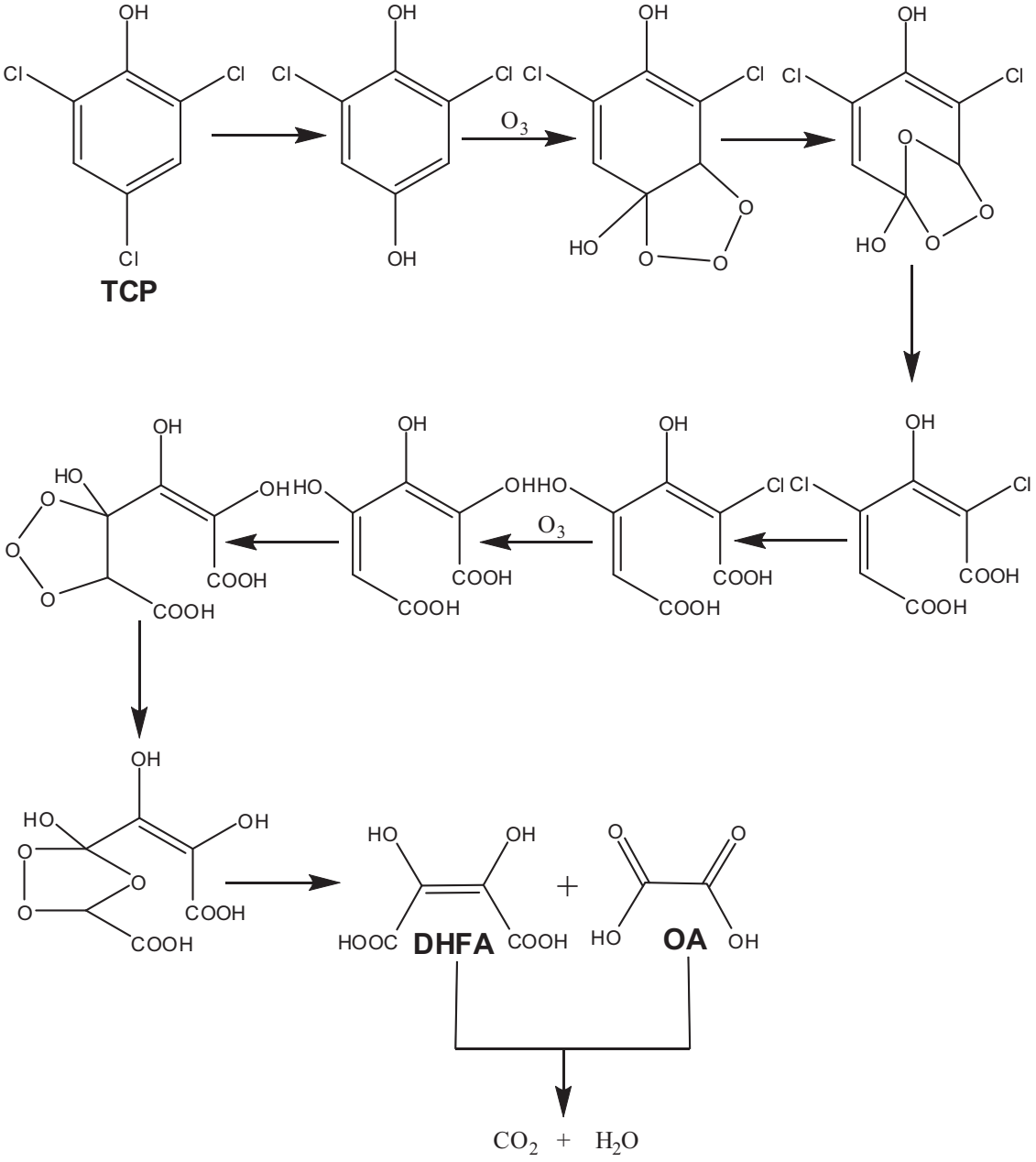

Scheme 1. Proposed mechanism: mechanism of the scheme.

catalysts. The structure and dispersion of the metal on the supports are affected by the preparation method, so good catalyst preparation process can significantly improve the catalytic activity. Currently, the supports for heterogeneous system are including Al_2O_3, SiO_2 and TiO_2; the active components are Ce, and Zr, due to the more acidic nature of the silica, 2.5% Ce–Zr/SiO_2 showed high catalytic conversion and selectivity toward the products among all the catalysts. The conversions and the selectivity toward products are in correlation with the acidic nature of the catalysts. The results show that the metal oxide supported catalysts give excellent activity during the ozone decomposition.

3.9. Mechanism

Molecular ozone is involved in oxidative process occurring on the heterogeneous catalyst surface. The catalytic process is affected by properties of catalyst, the target pollutants, and the pH value of solution; therefore, it becomes difficult to establish the reactive intermediates. It is proposed that primarily the catalyst facilitates the binding of the substrate on its active site and either molecular ozone or the ozone decomposed on the neighing sits attack the organic molecule. Secondly the active adsorptive site and combination with feed molecules to form active complexes at lower activation energy, enhances the oxidative degradation of dechlorination of the chlorinated organic molecule. And then, the intermediates can be further oxidized on the surface of catalysts, or desorbed to the aqueous solution to be oxidized by ozone or $^{\bullet}OH$.

Ozone and hydroxyl radical would be the reactive oxidant species [41]. Firstly, initial organic compound would be adsorbed on the surface of catalyst. Secondly, a strong negative charge would appear into the six or five-membered chelate ring at the surface. Lastly, the ozone or hydroxyl radical would oxidize the surface complex to give oxidation by-products either desorbed

in solution or still adsorbed at the surface catalyst. Essentially, due to the acidic nature of the catalysts act as adsorptive materials in this mechanism, combine with organics to form the chelate that can be degraded by ozone or OH radical. This mechanism can explain the catalytic ozonation system with the good adsorptive properties (Scheme 1).

Ernst et al. [42] proposed, the adsorption of organics on the catalyst's surface would not be necessary to provide the catalytic effect, moreover, the adsorption would probably inhibit the effect due to an overlaying of hydroxyl groups. The dissolved ozone adsorbs first on the catalyst's surface and then decomposes rapidly due to presence of hydroxyl surface groups. Due to decomposition of ozone, active atomic oxygen is produced and reacted with supports hydroxyl surface groups to form OH^- or O_2H^- anions which subsequently can react very fast with another O_3 to form OH radicals or O_2H radicals. This radical reacts subsequently with another ozone molecule to generate an O_3^- radical. It decomposes into oxygen and a free OH radical which can oxidize organic compounds either in solution or on the surface of the catalysts.

Thus, during the process of pollutants degraded by heterogeneous catalytic ozonation, when the interfacial reaction occurs, the characteristics of organics play the decisive role. The pH of solution affects the adsorption of organic pollutants on the catalyst surface; the adsorption is the rate controlling step of the interfacial reactions, which determines the removal degree of organic pollutants. For •OH.mechanism, the activity of catalysts is related with the surface properties of metal oxides, especially the surface Lewis acid sites playing the important role in the catalytic reaction.

A variety of intermediates, products were formed by several mechanism of the reaction of ozonation with chlorophenols. Only some studies have looked carefully at the examination of the reaction pathways and intermediates, and final products of chlorophenols with ozone [43]. Formation of chloride, hydroxylation products, such as TCP, carboxylic acids have been observed in the ozonation of trichlorophenols. After the electrophilic attack of ozone the aromatic ring was destroyed. Ozonation products with carbon-carbon double bonds, such as DHFA and OA can react with ozone (proposed mechanism). It was expected that the reaction products would be simple carboxylic acids.

4. Conclusions

In this work, we reported the transformation products arising from TCP oxidation using ozone with conversions and selectivity and probable mechanism is described. Ce–Zr supported on alumina, silica and titania were successfully prepared via wet impregnation technique. Characterization of the catalysts showed that Ce–Zr is very well dispersed on the surface of the supports and Ce–Zr exists as three different phases. As the Ce–Zr loading increased, the acidity of the catalysts decreased. Dihydroxyfumaric acid (DHFA) and oxalic acid (OA) were oxidation products. All the reactions products were dechlorinated ones, and further oxidation gave mineralized products, CO_2 and water. Metal oxide supported Ce–Zr catalysts are found to have good product selectivity for partial oxidation to DHFA and OA in water at pH 11. While the conversion efficiency of the support was $SiO_2 > TiO_2 > Al_2O_3$ in the presence of ozone molecule, 1% Ce–Zr loaded on silica catalysts registered lower conversion than 2.5% loaded.

Acknowledgements

Authors thank the University of KwaZulu-Natal for the financial support and other research facilities and iThemba LABS, Materials Research Department, South Africa for access to the facilities used for the research.

Appendix A. Supplementary data

Supplementary data associated with this article can be found, in the online version, at http://dx.doi.org/10.1016/j.apcatb.2013.05.012.

References

[1] (a) C. Cooper, R. Burch, Water Research 33 (1999) 3695–3700;
(b) J. Hoigne, H. Bader, Water Research 17 (2) (1983) 173–183.
[2] (a) R.J. Miltner, H.M. Shukairy, R.S. Summers, Journal American Water Works Association 84 (1992) 53–62;
(b) M. Hautaniemi, J. Kakkas, R. Munter, M. Trapido, Ozone: Science & Engineering 20 (1998) 259–282.
[3] F. Zuma, S.B. Jonnalagadda, Journal of Environmental Science and Health Part A 44 (1) (2009) 48–56.
[4] V.S.R.R. Pullabhotla, C. Southway, S.B. Jonnalagadda, Oxidation Communications 31 (2008) 98–107.
[5] V.S.R.R. Pullabhotla, S.B. Jonnalagadda, Journal of Advanced Oxidation Technologies 11 (2008) 445–454.
[6] V.S.R.R. Pullabhotla, S.B. Jonnalagadda, Oxyfunctionalisation of n-hexadecane with ozone in presence of metal loaded zeolites, in: Hand Book of Zeolites, Nova Science Publishers, Inc., New York, 2009, pp. 237–289 (Chapter 9).
[7] S.B. Jonnalagadda, P. Dachipally, Journal of Environmental Science and Health Part A 46 (8) (2011) 887–897.
[8] D. Marie, U. Von Gunten, Water Research 42 (1–2) (2008) 13–51.
[9] H. Staehelin, J. Hoigne, Environmental Science & Technology 19 (1985) 1206–1213.
[10] R.L. David, CRC Handbook of Chemistry and Physics, 72nd ed., CRC Press, Boston, 1991, pp. 8–27.
[11] Y. Lee, U. Von Gunten, Water Research 44 (2) (2010) 555–566.
[12] R. Munter, Proceedings of the Estonian Academy of Sciences, Chemistry 50 (2) (2001) 59–80.
[13] P.S. Bailey, Ozonation in Organic Chemistry. Vol. I. Olefinic Compounds, Academic Press, New York, 1978, pp. 7–13.
[14] R.E. Buhler, J. Staehelin, J. Hoigne, Journal of Physical Chemistry 88 (12) (1984) 2560–2564.
[15] U. Von Gunten, U. Pinkernell, Water Science and Technology 41 (7) (2000) 53–59.
[16] G.V. Buxton, C.L. Greenstock, W.P. Helman, A.B. Ross, Journal of Physical and Chemical Reference Data 17 (2) (1988) 513–886.
[17] E. Gilbert, Water Science and Technology 14 (8) (1982) 849–861.
[18] R. Munter, S. Preis, S. Kamenev, E. Siirde, Ozone: Science & Engineering 15 (2) (1993) 149–165.
[19] C.D. Adams, R.A. Cozzens, B.J. Kim, Water Research 31 (10) (1997) 2655–2663.
[20] K. Verschueren, Handbook of Environmental Data on Organic Chemicals, Van Nostrand Reinhold, New York, 1983.
[21] A.A. Meharg, J. Wright, D. Osborn, Science of the Total Environment 251 (2000) 243–253.
[22] B.G. Oliver, K.D. Nicol, Environmental Science & Technology 16 (8) (1982) 532–536.
[23] R.P. Schwarzenbach, E. Molnar-Kubica, W. Giger, S.G. Wakeham, Environmental Science & Technology 13 (11) (1989) 2154–2156.
[24] H. Wang, J.L. Wang, Applied Catalysis B: Environmental 77 (1–2) (2007) 58–65.
[25] R.G. Parag, B.P. Aniruddha, Advances in Environmental Research 8 (2004) 501–551.
[26] S.B. Jonnalagadda, V.S.R.R. Pullabhotla, S. Maddila, E.C. Chetty, International Journal of Chemistry 1 (1) (2012) 119–129.
[27] B. Kasprzyk-Hordern, M. Ziolek, J. Nawrocki, Applied Catalysis B: Environmental 46 (2003) 639–669.
[28] A. Rahman, V.S.R.R. Pullabhotla, S.B. Jonnalagadda, Catalysis Communications 9 (2008) 2417–2421.
[29] H. Einaga, S. Futamura, Journal of Catalysis 227 (2004) 304–312.
[30] E.C. Chetty, S. Maddila, V.B. Dasireddy, S.B. Jonnalagadda, Applied Catalysis B: Environmental 117–118 (2012) 18–28.
[31] B.M. Reddy, A. Khan, Y. Yamada, T. Kobayashi, S. Loridant, J.C. Volta, Langmuir 19 (2003) 3025–3031.
[32] B.M. Reddy, P. Lakshmanan, P. Bharali, P. Saikia, G. Thrimurthulu, M. Muhler, W. Grulner, Journal of Physical Chemistry 111 (2007) 10478–10483.
[33] S. Maddila, V.B. Dasireddy, S.B. Jonnalagadda, Applied Catalysis B: Environmental 138–139 (2013) 149–160.
[34] P. Bazin, O. Saur, O. Marie, M. Daturi, J.C. Lavalley, A.M. Le Govic, V. Harle, G. Blanchard, Applied Catalysis B: Environmental 119–120 (2012) 20–216.
[35] A. Iglesias-Juez, A. Martinez-Arias, M. Fernandez-Garcia, Journal of Catalysis 221 (2004) 148–161.
[36] Q. Yu, L. Liu, L. Dong, D. Li, B. Liu, F. Gao, K. Sun, L. Dong, Y. Chen, Applied Catalysis B: Environmental 96 (2010) 350–360.

[37] X. Wang, G. Lu, Y. Guo, Y. Xue, L. Jiang, Y. Guo, Z. Zhang, Catalysis Today 126 (2007) 412–419.
[38] A. Mattsson, C. Lejon, V. Stengl, S. Bakardjieva, F. Oplustil, P. Ola Andersson, L. Osterlund, Applied Catalysis B: Environmental 92 (2009) 401–410.
[39] E.C. Chetty, S. Maddila, C. Southway, S.B. Jonnalagadda, Industrial & Engineering Chemistry Research 51 (2012) 2864–2873.
[40] V.S.R.R. Pullabhotla, S.B. Jonnalagadda, Industrial & Engineering Chemistry Research 48 (2009) 9097–9105.
[41] B. Legube, N.K. Vel Leitner, Catalysis Today 53 (1999) 61–72.
[42] M. Ernst, F. Lurot, J.C. Schrotter, Applied Catalysis B: Environmental 47 (2004) 15–25.
[43] M. Pera-Titus, V. Garcia-Molina, M.A. Banos, J. Gimeneza, S. Esplugas, Applied Catalysis B: Environmental 47 (2004) 219–256.